



HAL
open science

Numerical simulations of flow and heat transfer in a wall-bounded pin matrix

Sofiane Benhamadouche, Imran Afgan, Remi Manceau

► **To cite this version:**

Sofiane Benhamadouche, Imran Afgan, Remi Manceau. Numerical simulations of flow and heat transfer in a wall-bounded pin matrix. *Flow, Turbulence and Combustion*, 2019, 10.1007/s10494-019-00046-8. hal-02179021v1

HAL Id: hal-02179021

<https://hal.science/hal-02179021v1>

Submitted on 10 Jul 2019 (v1), last revised 2 May 2020 (v2)

HAL is a multi-disciplinary open access archive for the deposit and dissemination of scientific research documents, whether they are published or not. The documents may come from teaching and research institutions in France or abroad, or from public or private research centers.

L'archive ouverte pluridisciplinaire **HAL**, est destinée au dépôt et à la diffusion de documents scientifiques de niveau recherche, publiés ou non, émanant des établissements d'enseignement et de recherche français ou étrangers, des laboratoires publics ou privés.

Numerical Simulations of Flow and Heat Transfer in a Wall-Bounded Pin Matrix

S. Benhamadouche · I. Afgan* · R.
Manceau

Received: date / Accepted: date

Abstract A detailed computational study was performed for the case of a wall-bounded pin-fin-array in a staggered arrangement, representative of industrial configurations designed to enhance heat transfer. In order to evaluate the level of turbulence modelling necessary to accurately reproduce the flow physics at three (3) different Reynolds numbers (3,000, 10,000 and 30,000), four models were selected: two eddy-viscosity URANS models (k - ω -SST and ϕ -model), an Elliptic Blending Reynolds-stress model (EB-RSM) and Large Eddy Simulation (LES). Global comparisons for the pressure loss coefficients and average Nusselt numbers were performed with available experimental data which are relevant for industrial applications. Further detailed comparisons of the velocity fields, turbulence quantities and local Nusselt numbers revealed that the correct prediction of the characteristics of the flow is closely related to the ability of the turbulence model to reproduce the large-scale unsteadiness in the wake of the pins, which is at the origin of the intense mixing of momentum and heat. Eddy-viscosity-based turbulence models have difficulties to develop such an unsteadiness, in particular around the first few rows of pins, which leads to a severe underestimation of the Nusselt number. In contrast, LES and EB-RSM are able to predict the unsteady motion of the flow and heat transfer in a satisfactory manner.

Keywords Large Eddy Simulation · Nusselt number · Pressure distribution · Pin-fin-arrays · Unsteady Reynolds-Averaged Navier-Stokes

S. Benhamadouche
EDF R&D, Fluid Mechanics, Energy and Environment Dept., 78401 Chatou, France
Tel.: +33-130-877986, E-mail: sofiane.benhamadouche@edf.fr

I. Afgan (*Corresponding Author)
Modelling and Simulation Centre, School of MACE, The University of Manchester, UK
Tel.: +44-161-2754334, E-mail: imran.afgan@manchester.ac.uk

R. Manceau
CNRS / Univ Pau & Pays Adour / E2S UPPA, Laboratoire de mathématiques et de leurs applications de Pau - Fédération IPRA, UMR5142, 64000, Pau, France and Inria Bordeaux-Sud-Ouest, project-team CAGIRE, E-mail: remi.manceau@univ-pau.fr

1 Introduction

Heat transfer augmentation has been an open question since the invention of the first Stirling engine in the early nineteenth century. Over the last 200 odd years various designs and techniques have been used to enhance the effective heat transfer between internal flow components such as heat transfer from a working fluid/solid to a passive fluid in solar thermal or nuclear applications. In thermal-hydraulics systems one of the main objectives is thus the effective heat transfer with minimum pressure drop across the working system. The current test-case consists of the flow through a wall-bounded pin matrix in a staggered arrangement with a heated bottom wall. In addition to the complex underlying flow physics, this case is close to several industrial configurations found in internal cooling of gas-turbine blades, electronic devices and nuclear thermal-hydraulics. The use of pin-fin-arrays has proved to be an effective technique in achieving enhanced rates of heat transfer in the past. Some of the earlier experimental studies done by Sparrow et al. (1980); VanFossen (1981); Metzger et al. (1982); Armstrong and Winstanley (1988) and more recently by Ames et al. (2005); Ames and Dovrak (2006a,b); Ames et al. (2007); Huang et al. (2018) report a number of flow characteristics including the heat transfer and pressure loss coefficients through various configurations of pin-fin-arrays.

Of particular interest among these are the experiments of Ames et al. (2005); Ames and Dovrak (2006a,b); Ames et al. (2007) which were chosen as test case for the 15th ERCOFTAC-SIG15/IAHR Workshop on Refined Turbulence Modelling held at Chatou in 2011. This particular test case was chosen for the workshop to assess and examine the suitability of various advanced modelling techniques/methods for flow and heat transfer calculations in complex, practice-relevant situations. The present work reported in this paper made a major contribution to this workshop and the full set of current results can be accessed through the ERCOFTAC Knowledge Base Wiki¹; later referred to as ERCOFTAC-KB-Wiki for simplicity. Various numerical studies conducted prior to the workshop, such as the Unsteady Reynolds-Averaged Navier-Stokes (URANS) calculations by Delibra et al. (2009); Hanjalić et al. (2005), and hybrid Reynolds-Averaged Navier Stokes/Large Eddy Simulation by Delibra et al. (2010) also formed the baseline for numerical contributions along with the experimental data of Ames et al. (2005); Ames and Dovrak (2006a,b); Ames et al. (2007) for the workshop.

The aim of the present study is to evaluate different strategies for modelling turbulence in the pin-fin-array test case of the workshop. Of particular importance is the determination of the level of modelling necessary to predict the main characteristics of the flow and heat transfer. In the past, URANS has been shown to be able to reproduce 2D and 3D wakes of bluff bodies (Durbin 1995; Iaccarino et al. 2003), but heat transfer predictions in complex flows close to industrial configurations, such as the wall-bounded pin matrix, are still very challenging. LES is undoubtedly a good candidate for reproducing the physics of such flows accurately, but at a cost unaffordable for high Reynolds numbers, such that comparing LES with lower-cost URANS methods, is of great interest to industry.

The present paper starts with the description of the experimental and numerical test cases (section 2), followed by discussion of numerical treatment given in

¹ http://www.kbwiki.ercoftac.org/w/index.php/Abstr:UFR_4-18

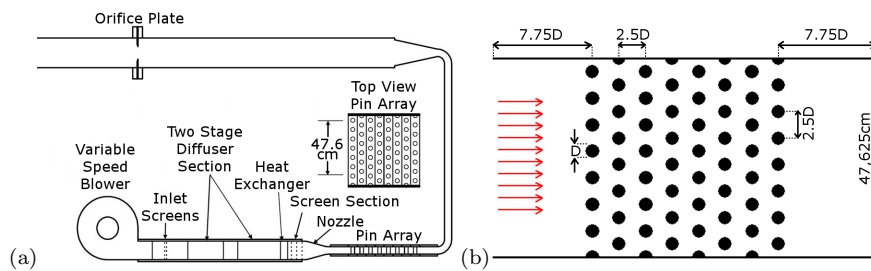


Fig. 1 2D sketch of Ames et al. (2007) experiment. (a) Complete experimental setup (b) Top view of the pin-fin configuration.

73 section 3. This will be followed by discussions of some of the main results in sec-
 74 tions 4 and 5; the full set of results can be found in the ERCOFTAC Knowledge
 75 Base Wiki²

76 2 Test Case Description

77 2.1 Experimental setup

78 The experiments of Ames et al. (2005); Ames and Dovrak (2006a,b) and Ames
 79 et al. (2007) were conducted in a small bench top wind tunnel for a staggered pin-
 80 fin-array consisting of 8 rows with $7\frac{1}{2}$ pins per row (see Figure 1). Both the cross
 81 passage (S/D) and stream-wise (X/D) pin spacing ratios were equal to 2.5 while
 82 the pin height to diameter (H/D) ratio was equal to 2. The pin diameter (D) was
 83 chosen to be equal to 2.54 cm. The test section began at $7.75D$ upstream of the
 84 centerline of the first row of pins and ended $7.75D$ downstream of the centerline
 85 of the last row. The inlet total temperature and static pressure were measured on the
 86 centerline, $5D$ upstream of row 1, whereas the exit static pressure was measured
 87 $5D$ downstream of row 8. Tests were conducted at three Reynolds numbers: 3,000,
 88 10,000, and 30,000 which were based on the maximum gap velocity (V_G) and the
 89 pin diameter (D). The gap bulk velocity was determined between two adjacent
 90 pins of the same row. The readers are referred to the ERCOFTAC-KB-Wiki for
 91 further details about the experimental setup, results and data uncertainties. The
 92 remaining description will focus on the numerical test-case which is studied and
 93 on the data utilized for the present comparisons.

94 2.2 Computational Setup

95 The computational domain shown in Figure 2(a), consisting of 8 by 2 pins, was
 96 used for all the simulations. The chosen domain is essentially a sub-domain of the
 97 experimental setup with the assumption of lateral (Y -axis) periodicity. All solid
 98 surfaces (pins, bottom and top walls) were set as no-slip solid walls. The inlet of
 99 the channel was set at a distance $L_U = 10D$ upstream of the center of the first

² http://www.kbwiki.ercoftac.org/w/index.php/Abstr:UFR_4-18

row of pins, whereas the outlet was $L_D = 15D$ downstream of the center of the last row of pins (this gives $X_{inlet} = -10D$ and $X_{outlet} = 32.5D$), respectively. Note that these two distances were both equal to $7.75D$ in the experimental setup but are not sufficient to perform reliable CFD calculations (see Afgan et al. (2007) and Parnaudeau et al. (2008)), in particular the upstream distance, unless one represents the nozzle of the experiment which would lead to added computational costs. On the other hand, the height of the computational model was set to match the experimental set-up, $H = 2D$.

For the computations, the temperature was treated as a passive scalar with an imposed temperature at the inlet, and an imposed heat flux at the bottom wall with adiabatic conditions elsewhere. For the Large Eddy Simulations (LES), a uniform inflow velocity was imposed without any synthetic or precursor turbulence generation. Note that the reported inflow turbulence intensity in the experiment was about 1.4%. In fact, different inlet conditions would have certainly affected the flow around the first and the second rows but not around the subsequent rows. On the other hand, for URANS a uniform velocity and 5% turbulence intensity were imposed at the inlet. This latter condition triggers the production of the Reynolds stresses, mandatory for their development. Some tests (not reported herein) which were carried out without inlet turbulence showed that the computations degenerate to a solution where the Reynolds stresses vanish. However, preliminary tests also showed that the level of inlet turbulence intensity only affects the flow around the first two rows and that a value of 5% leads to results in better agreement with the measurements. The inlet condition for the dissipation rate (ε) in URANS was given by the standard relation used for internal flows

$$\varepsilon = \frac{C_\mu^{3/4} k^{3/2}}{0.1\kappa H} \quad (1)$$

where k is the turbulent kinetic energy, $H = 2D$ (the height of the channel), $\kappa = 0.42$ and $C_\mu = 0.09$. Isotropy of turbulence is assumed at the inlet for the Reynolds-stress model.

For the computations, a Cartesian co-ordinate system was used with X , Y and Z -axes in the stream-wise, span-wise (lateral) and wall-normal directions, respectively. 1-D profiles were drawn along lines A1, B & C (see Figure 2(b)) for post-processing/comparisons. The main lines for the velocity components and the Reynolds stresses were A1 and B and the main line for the pressure coefficient was C (mid-span location). The exact positions of the lines were:

- **A1-** Line at mid-span ($Y/D = 0$) location between two adjacent pins of the same row along the channel height (Z -axis).
- **B-** Surface to surface line between two adjacent pins of the same row at mid channel height ($Z/D = 1.0$) along the lateral (Y) direction.
- **C-** Circumferential line around the pin surface from $0^0 - 180^0$, at mid channel height ($Z/D = 1.0$). Angle zero (0^0) on the leading edge of the pins with a counter-clockwise orientation.

The local Nusselt number is given by $Nu = q_w D / (\lambda(T_w - T_{ref}))$ where λ is the thermal conductivity, and T_w & T_{ref} are the time averaged temperatures at the wall and the reference value, respectively. T_{ref} takes into account the increase in the bulk temperature of the fluid from the heated surface as it flows down the

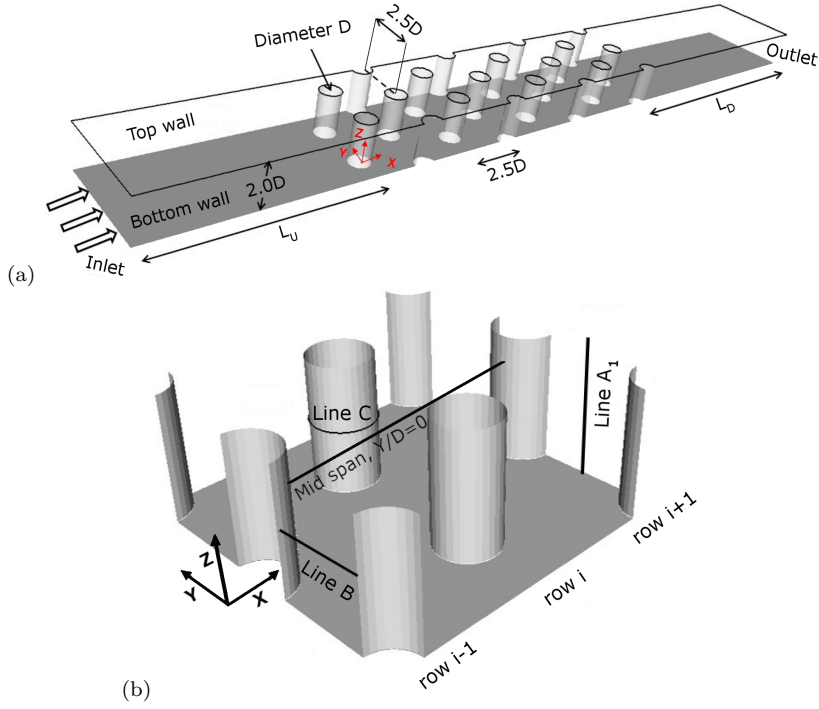


Fig. 2 (a) Sketch of the complete computational domain (b) Row numbering and lines (A1, B and C) locations. $i = 1, \dots, 8$. Line A1: ($X = 2.5D(i - 1)$, $Y = 0$ if i is even and $Y = 1.25D$ if i is odd, $0 \leq Z \leq 2D$). Line B: ($X = 2.5D(i - 1)$, $-0.75D \leq Y \leq 0.75D$ if i is even and $0.5D \leq Y \leq 2D$ if i is odd, $Z = D$). Line C : Centerline of the cylinder ($Z = D$), 0^0 at the leading edge (sense of rotation: counter clockwise with Z -axis from bottom to top wall).

144 array (see Nordquist (2006)). Therefore, at a given X location, one gets: $T_{ref} =$
 145 $q_w S_h(X) / (\rho C_p V_0 S_i)$, where $S_h(X)$ is the heated surface from the inlet to X .
 146 Nordquist (2006) used an estimate of this surface $S_h = (-X_{inlet} + X) S_{htot} / L_X$
 147 where X_{inlet} is the X coordinate of the inlet plane, S_{htot} the total heated surface
 148 (here the surface is from X_{inlet} to X_{outlet}) and L_X the total length of the domain
 149 ($L_X = X_{outlet} - X_{inlet}$). ρ , C_p and S_i are the fluid density, the specific heat and
 150 the inlet surface area, respectively.

151 3 Numerical Treatment and Models

152 3.1 General Description of the computations

153 All numerical simulations were performed using the Électricité de France (eDF)
 154 in-house open source solver *Code_Saturne* (<http://code-saturne.org>) (Archambeau
 155 et al. (2004)). The code is based on an unstructured collocated finite-volume ap-
 156 proach for cells of any shape. It uses a predictor/corrector method with Rhie and
 157 Chow interpolation (Rhie and Chow (1982)) and a SIMPLEC algorithm, (Ferziger
 158 and Perić (2012)) for the pressure correction. For LES, pure second-order central

Table 3.1.1 Experimental flow conditions. Reynolds number based on pin diameter (Re_D), inlet temperature (T_{inlet}), inflow velocity (V_0), fluid viscosity (ν), specific heat at constant pressure (C), thermal conductivity (λ), prescribed wall heat flux(q)

Re_D	$T_{inlet}(K)$	$V_0(m/s)$	$\nu(m^2/s)$	$C(J/kg/K)$	$\lambda(W/m/K)$	$q(W/m^2)$
3,000	300	1.06	0.000015	1005	0.0255	100
10,000	300	3.54	0.000015	1005	0.0255	300
30,000	300	10.62	0.000015	1005	0.0255	1000

159 differencing scheme was applied for the velocity components whereas for the tem-
 160 perature a central difference scheme with a slope test was used. Here the slope test
 161 determines whether to use a pure central scheme or to use first-order upwinding
 162 based on limiting of the overshoots. It is worth mentioning here that the slope test
 163 is done locally both in time and space. The time-advancing scheme was second-
 164 order, based on Crank-Nicolson/Adams Bashforth (the scheme for diffusion in-
 165 cluding the velocity gradient was totally implicit, for convection semi-implicit and
 166 for diffusion including the transpose of the velocity gradient explicit). For URANS,
 167 a centered scheme with a slope test was used for the velocity components and the
 168 temperature, whereas a first-order upwind scheme was utilized for the turbulence
 169 quantities. The time-advancing scheme in this case was first-order Euler which
 170 needs substantially smaller time steps for stability reasons. However, the use of
 171 the first-order Euler scheme here is justified as it is substantially faster than a
 172 second-order semi-implicit scheme such as the one used for the LES simulations.

173 Three Reynolds numbers were computed: $Re_D = 3,000$ only with LES, $Re_D =$
 174 $10,000$ with both LES and URANS and $Re_D = 30,000$ only with URANS. For
 175 the test cases the experimental flow conditions are listed in Table 3.1.1. For the
 176 computations a Prandtl number of 0.71 was used with fluid thermal conductivity
 177 defined as $\lambda = 1/(PrRe_D)$. The temperature was treated as a passive scalar with
 178 the inlet temperature set as 0^0 and the imposed heat flux set to unity. Zero-
 179 gradient boundary conditions were used for all the variables at the outlet and an
 180 implicit periodic condition was set in the lateral direction for all the variables. All
 181 the computations were run on EDF BlueGene/P and BlueGene/Q supercomputers
 182 using up to 4096 cores costing just under 3 million core Central Processing Unit
 183 (CPU) hours (approximately 45,000 kAU) for each LES simulation and around 2
 184 million (approximately 30,000 kAU) for each URANS simulation.

185 3.2 Turbulence models

186 The LES implementation in Code_Saturne (Benhamadouche 2006) is based on
 187 the dynamic Smagorinsky model (Germano et al. (1991)) with Lilly's minimiza-
 188 tion (Lilly (1992)) in which the Smagorinsky constant C_S is clipped below zero
 189 and above 0.065. This model has been successfully used for flows around bluff
 190 bodies and in turbo-machinery; please see the effect of clipping of C_S in Afgan
 191 et al. (2011). A turbulent Prandtl number of 0.5 was used when solving for the
 192 temperature with LES, see Grotzbach (2011).

193 In the current study three low Reynolds number URANS models were chosen
 194 based on their availability and relative popularity in the heat transfer community:

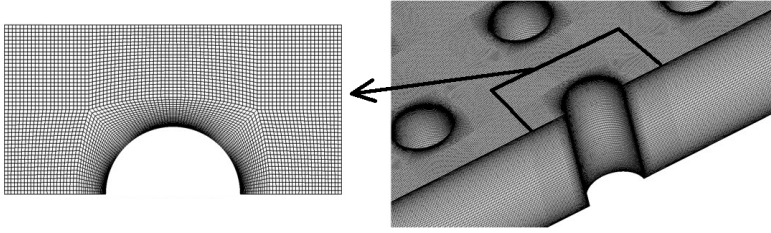


Fig. 3 Computational mesh used for LES at $Re_D = 3,000$.

195 the k - ω -SST model (Menter (1994)), the ϕ -model (Laurence et al. (2005)) and the
 196 EB-RSM model (Manceau (2015)).

197 The k - ω -SST model uses a blending between the standard $k - \omega$ and $k - \varepsilon$
 198 models. The ϕ -model uses the elliptic relaxation concept introduced by Durbin
 199 (1991). It is a stabilized version of the $\overline{v^2} - f$ model (Durbin 1995), based on the
 200 variable $\phi = \overline{v^2}/k$, where $\overline{v^2}$ characterizes the energy of the wall-normal fluctua-
 201 tions and is used in the evaluation of the eddy viscosity. For the present study, in
 202 both eddy-viscosity models, a Simple Gradient Diffusion Hypothesis (SGDH) was
 203 used for the temperature equation with a turbulent Prandtl number of 0.9.

204 The EB-RSM model proposed by Manceau and Hanjalić (2002) and later mod-
 205 ified by Manceau (2015) is inspired by the elliptic relaxation concept for the
 206 Reynolds stresses. Instead of using six relaxation equations, it solves one elliptic
 207 equation for a parameter α which is equal to zero at the wall and goes to
 208 1 far from the wall. This parameter is then used to blend near-wall and remote
 209 (away from the wall) regions for the redistribution and dissipation terms of the
 210 Reynolds-stress transport equations. In the current formulation the EB-RSM uses
 211 the Speziale, Sarkar and Gatski model (Speziale et al. (1991)) for the homoge-
 212 neous part of the redistribution term. For the temperature equation a Generalized
 213 Gradient Diffusion Hypothesis (GGDH) approach is used with a constant of 0.23.
 214 In the present simulations the use of more advanced models such as the AFM
 215 (Algebraic Flux Model), the EB-AFM or the EB-GGDH (Dehoux et al. 2012) did
 216 not affect the results for global quantities such as the mean Nusselt number. This
 217 suggests that in the forced convection regime, good predictions of heat transfer can
 218 be obtained with simple models for temperature diffusion as long as the dynamics
 219 of the flow is accurately resolved.

220 3.3 Computational meshes

221 Figure 3 shows the zoomed in views of the mesh used for LES at $Re_D = 3,000$.
 222 The mesh resolutions for the different computations are given in Table 3.3.2 (see
 223 table caption for details).

224 Note that for URANS, only the parameters used for the finest grid are men-
 225 tioned. The two coarser levels were obtained by coarsening the grid spacing by a
 226 factor of 2 in all the directions. Particular attention was paid to the grid refine-
 227 ment near the solid walls. Two meshes containing 18 million and 76 million cells
 228 were utilized in LES to simulate the two Reynolds numbers $Re_D = 3,000$ and
 229 $Re_D = 10,000$, respectively, ensuring that the non-dimensional wall distance of

Table 3.3.2 Mesh information. (*) Only the information of the finest meshes is given. Total number of cells in the domain (nb), number of cells around the pins in circumferential direction (nb_θ), number of cells in the wall normal (Z) direction (nb_z), normalized wall-adjacent cell size in the wall normal direction around the pins (n_θ/D), normalized wall-adjacent cell size in the wall normal direction-at the bottom wall (n_z/D), -at the top wall (n_{zh}/D).

<i>Computation</i>	nb	nb_θ	nb_z	n_θ/D	n_z/D	n_{zh}/D
LES $Re_D = 3,000$	18.2 million	176	90	0.0028	0.0065	0.0536
LES $Re_D = 10,000$	76.2 million	320	120	0.0015	0.0019	0.0584
URANS(*) $Re_D = 10,000$	17 million	128	112	0.00075	0.001	0.065
URANS(*) $Re_D = 30,000$	29 million	128	160	0.00025	0.00025	0.0625

230 the first computational cell (n^+) remained below 2 almost everywhere. Moreover,
 231 it was also carefully checked that the near-wall cells satisfy the usual refinement
 232 criteria. The current non-dimensional values of $y^+ \approx 2$ and $\Delta z^+ \leq 40$, clearly
 233 satisfy the resolved LES refinement criteria of $y^+ < 2$, $\Delta x^+ = 50 - 150$ and
 234 $\Delta z^+ = 15 - 40$, (Frohlich et al. 2005; Temmerman et al. 2003) (also see the wall
 235 treatment figures in the ERCOFTAC-KB-Wiki for further details).

236 An additional way to ensure that the mesh is sufficiently fine is to carry out
 237 simulations without using a subgrid-scale (sgs) model in order to quantify its
 238 effect on the solution. It was observed that the influence of the sgs model was very
 239 limited for the present level of mesh refinement (see the Sensitivity to the sub-grid
 240 scale model section and relevant figures in the ERCOFTAC-KB-Wiki for details).

241 3.4 Grid convergence study for URANS

242 A separate grid convergence study was performed for all the three URANS models
 243 at the two higher Reynolds numbers. Here only the study performed for $Re_D =$
 244 $10,000$ with the EB-RSM model is presented for the grid convergence study as
 245 conclusions for all other models were similar. Three levels of refinement were used
 246 for all the models as described before.

247 Figures 4a and 4b show the mean stream-wise velocity and the pressure co-
 248 efficient along the line B (pin mid-line) for the $Re_D = 10,000$ case for row 3,
 249 respectively. As the computations were unsteady, the *r.m.s.* values, or more gener-
 250 ally the Reynolds stresses were combined as the sum of the resolved and modelled
 251 parts: $R_{ij} = R_{ij}^{res} + R_{ij}^{mod}$. These modelled and resolved parts are not shown in the
 252 current paper but can be downloaded from the ERCOFTAC-KB-Wiki database.
 253 It is observed from figure 4 that the coarse mesh results are very far from the
 254 experiments. However, the two finest meshes only show slight difference in pro-
 255 files. Thus, the discussions in sections 4 and 5 are based on the results obtained
 256 with the finest mesh (called here “very fine mesh”). In order to gain confidence in
 257 the finest mesh results, a further sensitivity study on the numerical discretization
 258 schemes with and without slope test was also performed. Based on the results it
 259 was concluded that the use of a centered scheme for the turbulent quantities did
 260 not affect the results. Other tests were also carried out such as introducing outer
 261 iterations for pressure/velocity coupling but none of them exhibited a noticeable
 262 effect on the results and are hence not reported here (please see the Sensitivity

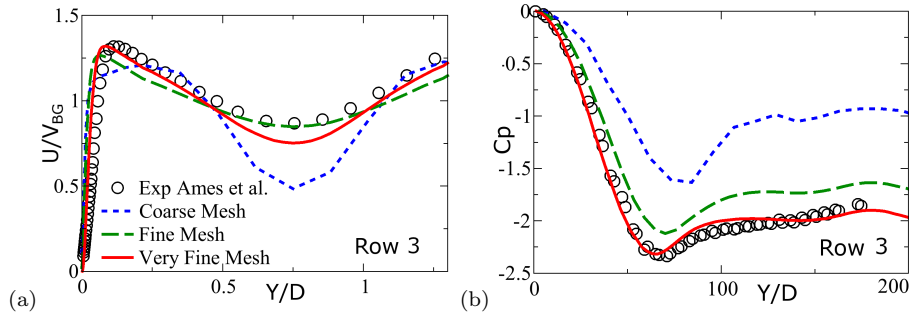


Fig. 4 Grid convergence study: Mean stream-wise velocity and mean pressure coefficient profiles along the pin mid-line (Line-B) obtained using EB-RSM at $Re_D = 10,000$.

Table 3.4.3 Parameters of the main computations which are reported in the current paper. Where $Timestep^+$ is the non-dimensional time step, Tot_{Pass} the number of total flow through passes and Ave_{Pass} is the number of passes over which the flow statistics were averaged.

<i>Test – case</i>	Re_D	V_{BG}	V_0	$Timestep^+$	Tot_{Pass}	Ave_{Pass}	\overline{CFL}_{max}
<i>LES DynSmag</i>	3,000	2.02	1.21	0.0015	39	16	0.8
<i>LES DynSmag</i>	10,000	6.18	3.71	0.0002	11	7	0.8
<i>EB – RSM</i>	10,000	6.18	3.71	0.001	43	20	1.8
ϕ – model	10,000	6.18	3.71	0.001	44	36	1
<i>k-ω-SST</i>	10,000	6.18	3.71	0.001	43	32	1.3
<i>EB – RSM</i>	30,000	18.53	11.12	0.0000625	11	9	0.6
ϕ – model	30,000	18.53	11.12	0.00025	19	14	0.9
<i>k-ω-SST</i>	30,000	18.53	11.12	0.00025	22	16	1.8

263 study to convection scheme on the ERCOFTAC-KB-Wiki database for detailed
264 plots).

265 Table 3.4.3 summarizes the main computations for which results are reported
266 in sections 4 and 5. Note that all simulations were run for a substantially long
267 period of time for the flow to fully develop. For the simulations a complete flow
268 through pass was defined based on the time the flow took from the inlet of the
269 domain to the outlet, T_{Pass} . Based on this, the total number of passes over which
270 each of the individual cases were run ($Tot_{Pass} = Total\ Simulation\ time / T_{Pass}$)
271 and the number of passes over which the flow statistics were averaged (Ave_{Pass}),
272 are given in table 3.4.3. The maximum local CFL number for each of the cases is
273 also given in the same table which is less than 1 for all LES simulations and less
274 than 2 for URANS.

275 4 Results and Discussions (Global Quantities)

276 4.1 Pressure loss coefficient

277 In this section we discuss the measured values of the pressure loss coefficient in
278 Ames et al. experiments as well as those obtained from the current numerical
279 simulations at the three computed Reynolds numbers. The pressure loss coefficient

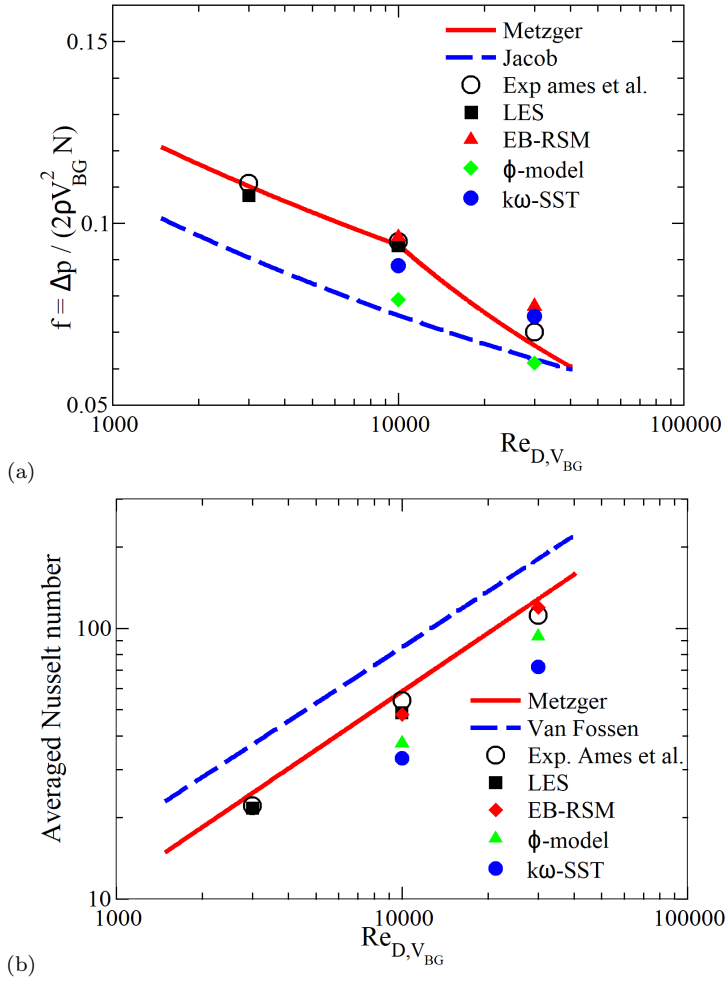


Fig. 5 (a) Pressure loss coefficient (b) Average Nusselt number at the bottom wall.

280 is based on the total pressure drop from the inlet to the outlet of the domain and
 281 is defined as $f = \Delta P / (2\rho V_{BG}^2 N)$, where N is the number of rows.

282 Figure 5a shows the computed pressure loss coefficient comparison with the
 283 measured values of Ames et al. and correlations of Jacob (1938) and Metzger
 284 et al. (1982)

285
 286 Jacob (1938):

$$287 \quad f = (0.25 + 0.1175/(P/D - 1)^{1.08})Re^{-0.16}$$

288 Metzger et al. (1982):

$$289 \quad f = 0.317Re_D^{-0.132} \text{ for } Re_D < 10^4$$

$$290 \quad f = 1.76Re_D^{-0.318} \text{ for } Re_D > 10^4$$

291 Table 4.1.1 compares various computations to the experiments and gives the
 292 relative errors. LES shows a very good agreement with the Metzger et al. (1982)

Table 4.1.1 Pressure loss coefficient for the different computations compared to Ames et al. experimental values.

$Re_D = 3,000$	Exp..	<i>LES</i>			
Value	0.111	0.1076			
Error (%)	-	3			
$Re_D = 10,000$	Exp.	<i>LES</i>	<i>EB - RSM</i>	ϕ	<i>k-ω-SST</i>
Value	0.095	0.0939	0.0963	0.0789	0.0883
Error (%)	-	1	1	17	7
$Re_D = 30,000$	Exp.	<i>EB - RSM</i>	ϕ	<i>k-ω-SST</i>	
Value	0.07	0.0771	0.0615	0.0744	
Error (%)	-	10	12	6	

293 correlation and Ames et al. experimental results. The relative error is equal to
 294 1% and 3% for the two computed Reynolds numbers, respectively. The EB-RSM
 295 model shows a satisfactory pressure loss coefficient at $Re_D = 10,000$ (1% error)
 296 but the result is worse at $Re_D = 30,000$ (where the error is 10%). The *k- ω -*
 297 *SST* model also exhibits globally good results (7% and 6% errors). On the other
 298 hand the ϕ -model gives the worst results with errors of 17% and 12% for the
 299 two Reynolds numbers, respectively. This will be further explained in section 5.2
 300 later. Wall resolved LES can thus be seen as an excellent candidate to obtain
 301 satisfactory pressure loss coefficients in the present configuration. It is important
 302 to note here that although the *k- ω -SST* model exhibits good results for the pressure
 303 loss coefficient, the physics of the present flow is not properly captured as will be
 304 shown later and thus one cannot rely on this model.

305 4.2 Average Nusselt Number Comparisons

306 Figure 5b shows all comparisons between simulations, experiments provided by
 307 Ames et al. and the correlations of VanFossen (1981) and Metzger et al. (1982).

$$308 \text{ VanFossen (1981): } Nus = 0.153Re^{0.686}$$

$$309 \text{ Metzger et al. (1982): } Nus = 0.079Re^{0.717}$$

310 Note that the local experimental results have an uncertainty of $\pm 12\%$, $\pm 11.4\%$,
 311 and $\pm 10.5\%$ for the 3,000, 10,000, and 30,000 Reynolds numbers, respectively, in
 312 the end-wall regions adjacent to the pins and $\pm 9\%$ away from the pins. For the
 313 simulations, the total area of the bottom wall was used for the calculation of the
 314 average Nusselt number.

315 Table 4.2.2 compares the computations with the experiments and gives the rel-
 316 ative errors. One can see that the two models using an eddy-viscosity (ϕ -model and
 317 *k- ω -SST*) are quite far from the experimental results, except for the ϕ -model at
 318 $Re_D = 30,000$. However, as will be shown later, this model exhibits wrong physics.
 319 LES and EB-RSM yielded satisfactory values within the experimental error inter-
 320 val. The superiority of these two models will be discussed later when showing the
 321 results of the local normalized Nusselt number on the bottom wall. Ames and
 322 Dovrak (2006a) using standard Realizable *k- ε* and RNG *k- ε* models also found

Table 4.2.2 Average Nusselt number comparison on the bottom wall for $Re_D = 3,000$ (Exp.-Ames et al., DLES-Delibra et al. (2010), URANS*-Delibra et al. (2009)).

$Re_D = 3,000$		Exp.	<i>LES</i>					
Value		22.1	21.6					
Error (%)		-	2					
$Re_D = 10,000$		Exp.	<i>LES</i>	<i>DLES</i>	<i>EB-RSM</i>	ϕ	<i>k-ω-SST</i>	URANS*
Value		54.1	48.6	44.1	48.1	37.6	33.1	46.2
Error (%)		-	10	18	11	30	39	14
$Re_D = 30,000$		Exp.	<i>EB-RSM</i>		ϕ	<i>k-ω-SST</i>	URANS*	
Value		111.5	114.8		93.3	72	122.3	
Error (%)		-	3		16	35	9	

323 a substantial underestimation of the average Nusselt number when the pins were
 324 heated. Delibra et al. (2009) used the URANS $\zeta - f$ model (which is very similar
 325 to the ϕ -model utilized in the present work) at the 10,000 and 30,000 Reynolds
 326 numbers and obtained average Nusselt numbers of 46.2 and 122.3, respectively.
 327 These values are also substantially different from the experimental results but it
 328 should be mentioned here that these values were obtained by using an imposed
 329 constant temperature at the wall. Using this boundary condition in the present
 330 work with the ϕ -model also led to higher values of the average Nusselt numbers (41
 331 and 100, respectively, not shown here). This shows that imposing the temperature
 332 gives higher Nusselt numbers than the ones obtained by imposing the heat flux
 333 with this model. The effect of the temperature boundary condition was also tested
 334 with the LES at $Re_D = 10,000$ and with the EB-RSM model at $Re_D = 30,000$.
 335 The average Nusselt numbers were found to be equal to 46 and 115.2, respec-
 336 tively. Hence, clear conclusions concerning the effect of imposing the temperature
 337 instead of the heat flux at the bottom wall can be drawn for these two models
 338 which gave more realistic physics than the eddy-viscosity models. However, one can
 339 state that there is clearly a strong influence of the thermal boundary conditions
 340 on the results. Delibra et al. (2008) also reported LES computations. However,
 341 the one carried out for $Re_D = 30,000$ was fairly coarse with a short integration
 342 time and will thus not be considered here for comparisons. Furthermore, their LES
 343 at $Re_D = 10,000$ gave an average Nusselt number of 44.3 with an error of 18%
 344 compared to the experiments of Ames et al. This led Delibra et al. (2010) to test a
 345 hybrid RANS/LES approach but the results were still less accurate than the ones
 346 obtained with their URANS approach based on the $\zeta - f$ model (see table 4.2.2).

347 5 Results and Discussions (Local Quantities)

348 5.1 Mean velocity

349 Figure 6 displays the dimensional mean stream-wise velocity field in the mid-plane
 350 ($Z = D$). The wakes downstream of the cylinders are similar in LES and EB-RSM
 351 and are shorter downstream of the cylinders from row 4 on-wards. This was not

352 observed at all for the ϕ -model and the k - ω -SST model. Furthermore, both eddy-
353 viscosity models (EVM) over-predicted the pin adjacent gap velocities. One can
354 thus conclude at this stage that the tested EVM models are not able to predict
355 the present flow. Clearly, they predict too long and too weak recirculation regions
356 behind the pins. It is well known that, in the case of wakes of infinite cylinders
357 (Durbin 1995) or wall-mounted obstacles (Iaccarino et al. 2003), the RANS models
358 (steady state computations) cannot accurately predict the recirculation region,
359 and that URANS can drastically improve the prediction by resolving a significant
360 part of the large-scale unsteadiness, which is a major contributor to the mixing
361 of momentum. It can be anticipated that the main difference between the EB-
362 RSM and the eddy-viscosity models lies in the tendency of the latter to provide a
363 steady solution because of their strongly diffusive character. It can also be argued
364 that eddy-viscosity models tend to overestimate turbulent production close to
365 stagnation points and thus overestimate the turbulent energy in the boundary
366 layers around the cylinders and, consequently, in their wake. This hypothesis will
367 be investigated below.

368 Figure 7 shows the mean axial velocity component along line B of rows 3 and 5
369 for the different computations (for further row comparisons see the ERCOFTAC-
370 KB-Wiki database). One observes from figure 7b that the EB-RSM model and
371 LES predictions are very close to each other. In fact, for row 3, the EB-RSM
372 model captures the near wall behavior even better than LES, as the peak value
373 by LES is slightly overpredicted. For row 5, both LES and the EB-RSM model
374 slightly overpredict the mean velocity near the pin. On the other hand, the eddy-
375 viscosity models fail to capture the near-wall and the inter-gap flow behavior, see
376 the underprediction at $Y/D = 0.1$ and $Y/D = 0.75$ in figure 7b, particularly for
377 the row 3 profile.

378 It is further observed that the two eddy-viscosity models exhibit a dramatic
379 deficit of the mean axial velocity midway between the tubes, in accordance to the
380 overestimation of the size of the recirculation regions as first observed in figure 6.
381 On the other hand, LES and EB-RSM models perform well compared to the exper-
382 imental data with a slight overestimation of the mean stream-wise velocity peaks
383 close to the walls at several locations, in particular starting from row 3. Note that
384 the convergence study shown in section 3 proved that the refinement needed to
385 obtain a convergent solution around pin 2 is very important (with the first two
386 levels of refinement, a deficit in the central velocity was observed). This is an in-
387 dication that the accurate reproduction of the large-scale unsteadiness is crucial
388 in this flow: Lardeau and Leschziner (2005) showed that the correct reproduction
389 of the unsteadiness of the wake of an obstacle requires a careful elimination of
390 sources of numerical diffusion. This remark suggests that the origin of the failure
391 of the eddy-viscosity models is in their inability to reproduce realistic large-scale
392 unsteadiness.

393 Figure 8 shows the mean axial velocity component along line A1 for the highest
394 Reynolds number case. It is observed that the two eddy-viscosity models severely
395 underestimate the mean streamwise velocity, supporting the earlier observations
396 made from figures 6 and 7. Both EVM models overpredict the length of the recir-
397 culation region behind each pin, such that the recovery of the boundary layer in
398 between the subsequent pins is slowed down. In contrast, the RSM model provides
399 a solution very close to the experimental profiles but slightly underestimates the
400 velocity all along the A1 line. However, this must not be interpreted as a deficit

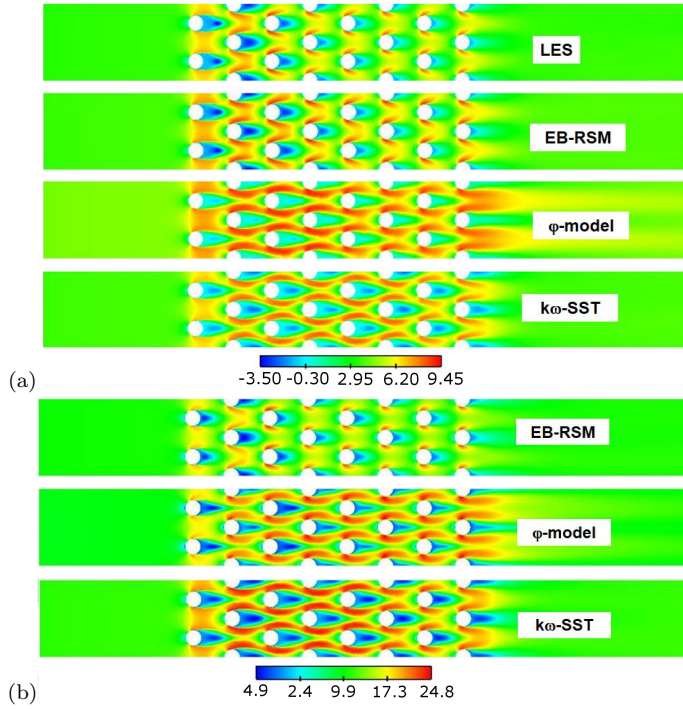


Fig. 6 Dimensional mean stream-wise velocity (m/s) in the mid-plane $z = D$ (a) $Re_D = 10,000$ (b) $Re_D = 30,000$.

401 of flow rate, which is conserved as the velocity underestimations on line A1 are
 402 compensated by overestimations elsewhere.

403 5.2 *r.m.s* Velocity

404 The best way to gain insight into the very different behavior of the models is to
 405 investigate the relative contributions of the resolved and modelled parts of the
 406 velocity field to the total *r.m.s* velocities, as shown in figure 9. Here, the contri-
 407 bution of the subgrid scales is neglected for LES (as it is not explicitly evaluated
 408 in the present Smagorinsky model formulation). Since no synthetic turbulence is
 409 prescribed at the inlet, there is no resolved content before the first pin, and the
 410 resolved contribution rapidly develops after the first row. However, as observed
 411 from the figure, the flow reaches a fully developed state only around the last row,
 412 in accordance with the experiments. The EB-RSM model also exhibits a rapid
 413 development of the resolved motion, with *r.m.s* levels of the same order of mag-
 414 nitude as those of LES. In addition, a smaller, but significant level of modelled
 415 stress contributes to the total fluctuations.

416 From figure 9 it is further observed that the behavior of the two eddy-viscosity
 417 models (EVM) is completely different from LES and EB-RSM. For the EVM
 418 cases, the contribution of the resolved motion remains small compared to that of

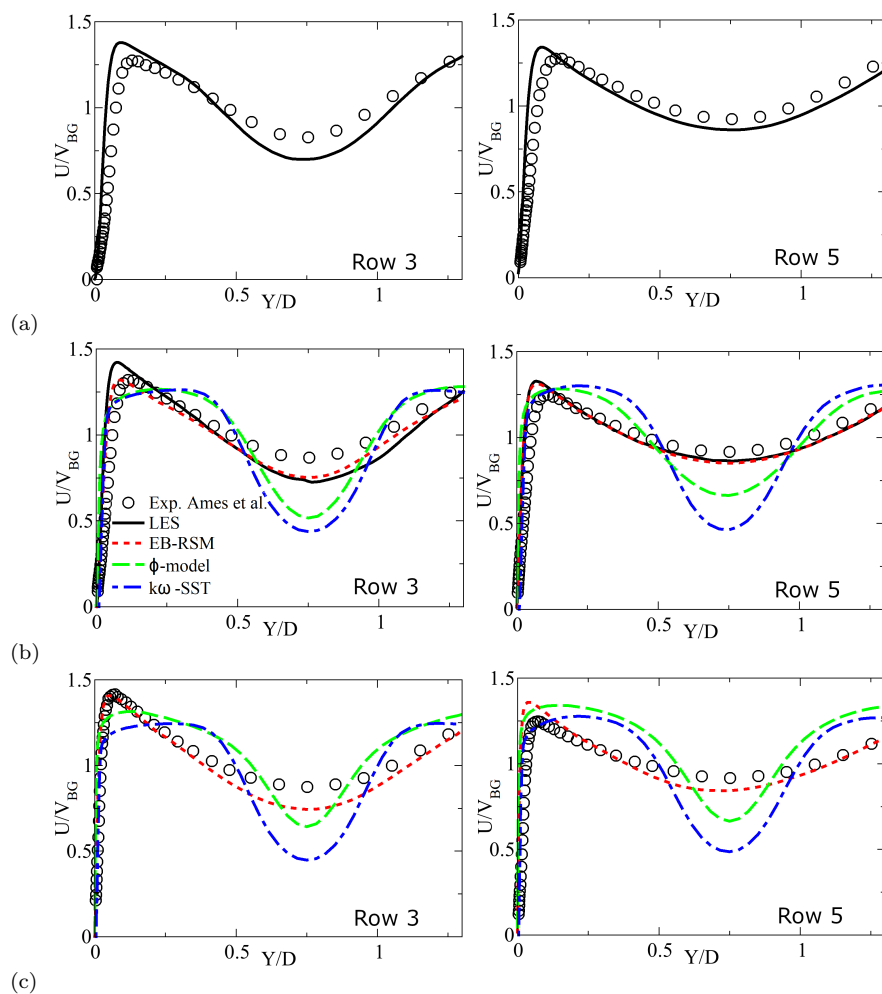


Fig. 7 Mean stream-wise velocity component along line B - LES and URANS computations (a) $Re_D = 3,000$ (b) $Re_D = 10,000$ (c) $Re_D = 30,000$.

419 the modelled motion, up to at least row 4 and even up to row 7 for the $k\text{-}\omega\text{-SST}$
 420 model. This result indicates that these models face difficulties to reproduce un-
 421 steadiness in the wake. As mentioned above, predicting the correct level of mixing
 422 in wakes dominated by large-scale vortex shedding, such as behind cylinders or
 423 wall-mounted obstacles (Durbin 1995; Iaccarino et al. 2003), requires a URANS
 424 solution with a very significant amount of resolved unsteadiness. This is the reason
 425 why the two eddy-viscosity models exhibit longer recirculation regions in figure 6
 426 and consequently underestimate the mean stream-wise velocity in between the
 427 subsequent pins (figures 7 and 8). Note that at $Re = 30,000$, the ϕ -model remains
 428 steady all the way down to the last row. It is interesting to remark here that with a
 429 coarser mesh (not shown here), the ϕ -model rapidly developed unsteadiness. This
 430 is in agreement with the findings of Fadai-Ghotbi et al. (2008); in coarse RANS

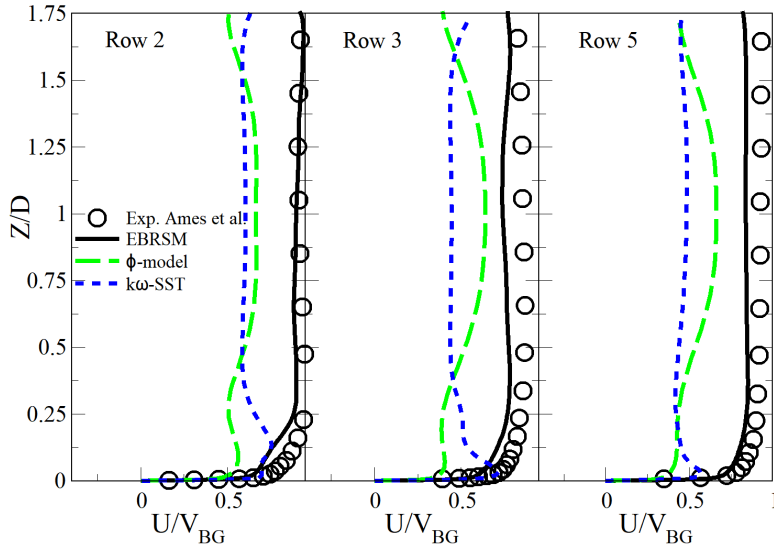


Fig. 8 Mean stream-wise velocity component along line A1 - URANS computations at $Re_D = 30,000$.

431 simulations, dispersive numerical errors (oscillations) can trigger an unsteady be-
 432 havior, which can paradoxically improve the predictions. The present results show
 433 that on fine-enough grids, the solution of eddy-viscosity models remains steady for
 434 the first rows and only gradually develops unsteadiness on subsequent rows.

435 This difficulty to develop an unsteady content, compared to the EB-RSM, can
 436 be attributed to an overestimation of diffusion in the wake that prevents the growth
 437 of resolved fluctuations. A first possible explanation would be that turbulence is
 438 generated in excess by EVM models in the region of the stagnation point (Taulbee
 439 and Tran 1988; Durbin 1996). For example, it is clear from Fig. 9, in the right-hand
 440 column, that the ϕ -model produces a high level of turbulence upstream of the first
 441 cylinder. Convection of this turbulence downstream may cause an overestimation
 442 of the turbulent diffusion in the wake. However, this stagnation point anomaly is,
 443 at least, partially corrected in the k - ω -SST model by the introduction of a produc-
 444 tion limiter: $P = \min(P_k, 10\varepsilon)$, where $P_k = 2\nu_t S_{ij} S_{ij}$ is the standard production
 445 term derived from the Boussinesq relation (Menter et al. 2003). Indeed, Fig. 9
 446 shows that this model does not exhibit the same overestimation of turbulence produc-
 447 tion as the ϕ -model in the stagnation region. Therefore, another explanation is
 448 more convincing, even if the two problems can be combined: it appears in Fig. 9,
 449 particularly for the SST model, that the overestimation of production takes place
 450 mainly in the wake of the cylinders. Indeed, as shown by Carpy and Manceau
 451 (2006) for the case of a periodic flow (synthetic jet), the Boussinesq relation used
 452 in eddy-viscosity models, i.e., the linear relation between the turbulent anisotropy
 453 tensor and the mean strain tensor, is at the origin of a strong overestimation of
 454 the modelled turbulent production, and, consequently, of the modelled turbulent
 455 diffusion of momentum, when the deformation varies rapidly in space or time and
 456 the Reynolds stress tensor does not have time to follow this evolution. This over-

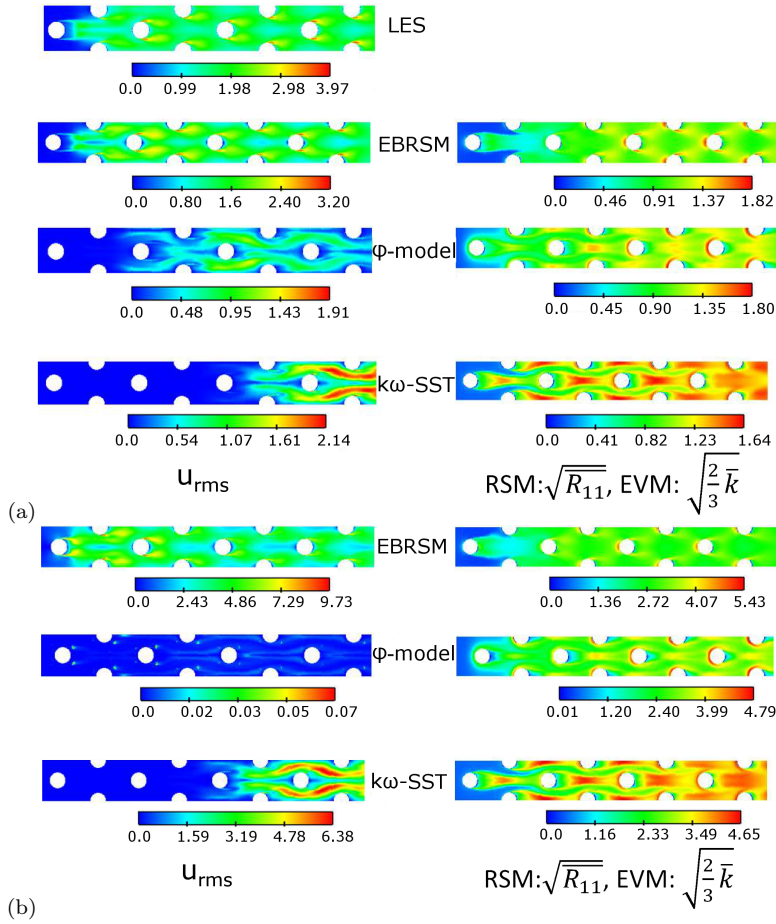


Fig. 9 Resolved (left) and modelled (right) contributions to the dimensional *r.m.s* of the stream-wise velocity component (m/s) in the mid-plane ($Z = D$)- LES and URANS computations (a) $Re_D = 10,000$ (b) $Re_D = 30,000$.

457 production bears some similarity to the problem of the stagnation point anomaly,
 458 since it is also to be traced to the use of the linear Boussinesq relation, but is
 459 active in other situations, far from the wall, when turbulence is out of equilibrium
 460 (see Hadžić et al. (2001), Hamlington and Dahm (2009) and Revell et al. (2011)).
 461 For instance, in a 2D-flow, it can be easily shown (Carpy and Manceau 2006) that
 462 the exact production of turbulent energy involves a factor of $\cos(2\Theta)$, where Θ is
 463 the angle between the eigenvectors of the anisotropy tensor and those of the strain
 464 tensor (*stress-strain lag*), such that eddy-viscosity models, which assume $\Theta = 0$,
 465 overestimate production. This can be generalized to 3D-flows by considering the
 466 so-called stress-strain lag parameter $C_{as} = -a_{ij}S_{ij}/\sqrt{2S_{ij}S_{ij}}$ (Revell et al. 2011).
 467 In the case of 2D tube bundles, a case very similar to the present pin-fin-array, it
 468 was shown, using experimental data of Simonin and Barcouda³, that the stress-

³ <http://cfd.mace.manchester.ac.uk/ercoftac>, case 78

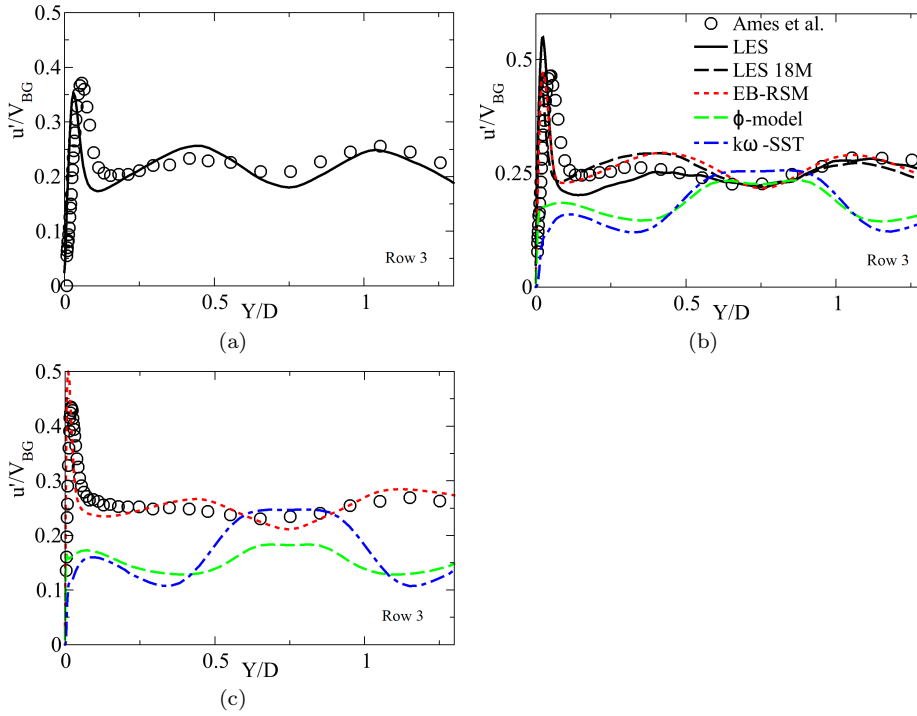


Fig. 10 *r.m.s.* of the stream-wise velocity component along line B - LES and URANS computations for row 3 (a) $Re_D = 3,000$ (b) $Re_D = 10,000$ (c) $Re_D = 30,000$.

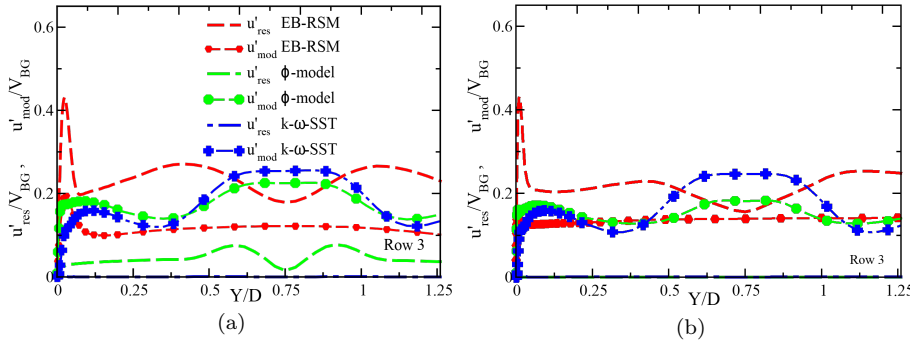


Fig. 11 Resolved, u'_{res} and modelled, u'_{mod} contributions to the *r.m.s.* of the stream-wise velocity component along line B - URANS computations (a) $Re_D = 10,000$ (b) $Re_D = 30,000$.

469 strain misalignment is so strong that large regions of negative production ($\Theta > 45$
 470 deg) are observed in between subsequent tubes (see Fig. 2.17 of Viollet et al. 1998).
 471 The lack of consideration of this stress-strain lag prevents the large-scale unsteadiness to be captured in cylinder wakes (Revell et al. 2011), a problem that can be
 472 avoided by using a Reynolds-stress model (Carpay and Manceau 2006).
 473

474 Figure 10 shows the *r.m.s.* profiles of the stream-wise velocity along line B.
 475 Here again only the profiles along row 3 are shown and the remaining profiles
 476 can be accessed via the ERCOFTAC-KB-Wiki database. The quantity plotted in
 477 the figure is $u' = \sqrt{u_1'^2 + \overline{R_{11}}}$, where u_1' is the resolved streamwise velocity fluctuation
 478 and $\overline{R_{11}}$ the time-averaged value of the stream-wise modelled Reynolds
 479 normal stress R_{11} . LES and EB-RSM models perform very well compared to the
 480 experimental data. As mentioned earlier, it can be seen in Fig. 11 that for the
 481 stream-wise stresses, a major part of the total fluctuations of the EB-RSM model
 482 comes from the resolved part, which again shows that this model easily repro-
 483 duces the large-scale unsteadiness appearing in the wake of the pins. However,
 484 in contrast with LES, the modelled part is not negligible. Figure 10 shows that
 485 the eddy-viscosity models severely underestimate the total stream-wise fluctua-
 486 tions, except in the central region. It is not expected from these models to provide
 487 very accurate *r.m.s.* velocities, since they are based on the Boussinesq relation,
 488 which is not designed to reproduce the individual normal stresses. However, the
 489 amplitude of u' is underestimated by a factor of more than 2 close to the pin sur-
 490 faces, which shows that a significant amount of turbulent energy is missing in this
 491 region. Figure 11 and more prominently the contours of Fig. 9 provide a rather
 492 enlightening explanation for this result. In contrast to the cylinder wake (regions
 493 far from the wall), where, as mentioned above, eddy-viscosity models yield a high
 494 level of modelled turbulent energy, it can be seen that the contribution of the
 495 modelled part close to the pin surfaces is of the same order of magnitude as that
 496 of the EB-RSM, but the *resolved content* remains very small, such that the to-
 497 tal, including the resolved and modelled parts, is significantly underestimated. In
 498 particular, the near-wall peak, which is largely contributed by the resolved part
 499 for the EB-RSM, is completely missed by the eddy-viscosity models. This result
 500 is of course consistent with the contourplots of Fig. 9, and definitely supports the
 501 conclusion that the main issue with the eddy-viscosity models is their difficulty to
 502 grow unsteadiness in the wake of the pins, due to their over-diffusive character.

503 5.3 Mean pressure coefficient

504 Figure 12 shows the profiles of the mean pressure coefficient along the midline
 505 of pins 3 and 5 for the three Reynolds numbers. Profiles along other pins can
 506 be accessed via the ERCOFTAC-KB-Wiki database. Note that the experimental
 507 results have an uncertainty of ± 0.075 at $Re_D = 3,000$ and of ± 0.025 at $Re_D =$
 508 $10,000$ and $Re_D = 30,000$. LES results are in relatively good agreement with the
 509 experimental data. EB-RSM exhibits overall satisfactory results as well. In fact for
 510 $Re_D = 10,000$ for Row 3, the EB-RSM prediction is even better than LES. This
 511 result is surprising at first glance, but it is important to emphasize that the LES
 512 does not have any fluctuating content at the inlet. Therefore, it takes some rows
 513 for the resolved turbulent energy to reach a level compatible with the experiments,
 514 in contrast to the EB-RSM for which the turbulence intensity at the inlet is 5%.
 515 This discrepancy is not observed at row 5, since the resolved energy content in the
 516 LES has developed.

517 On the other hand, both the eddy-viscosity models show less accurate results,
 518 in particular the ϕ -model. This is expected since the mean flow characteristics are

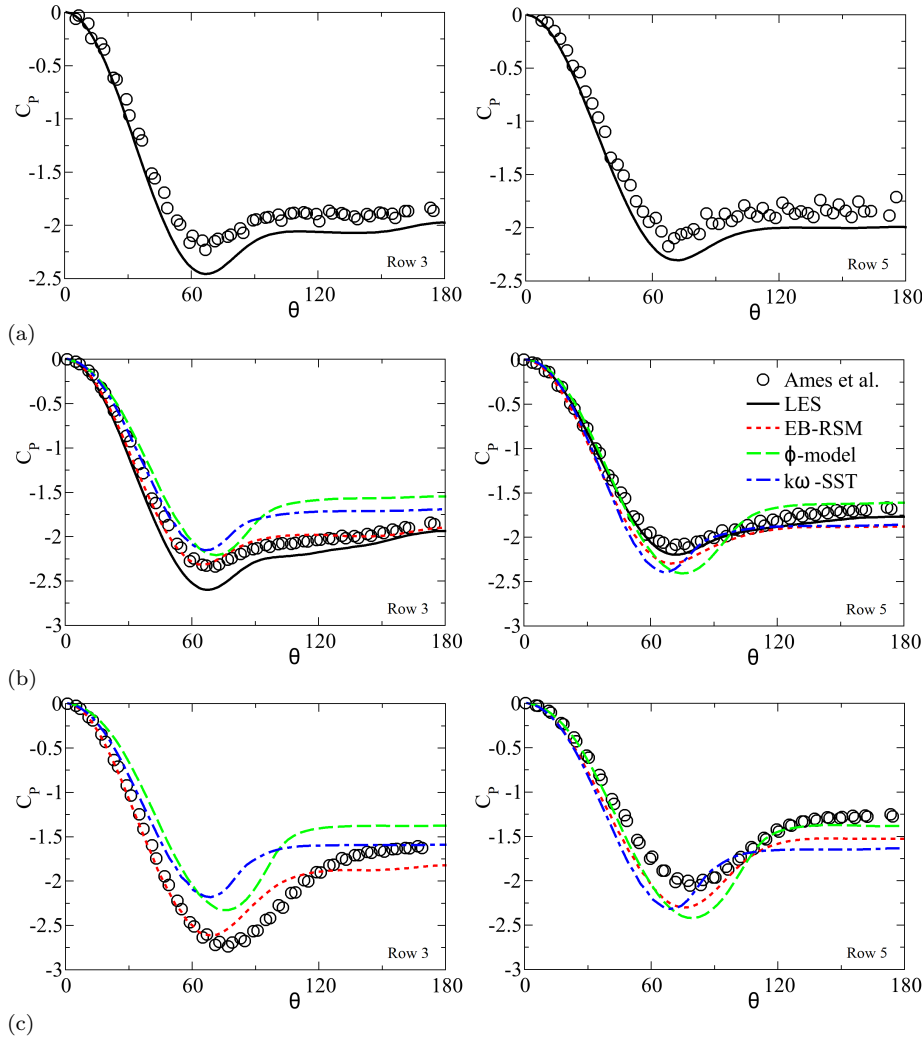


Fig. 12 Pressure coefficient along the line C- LES and URANS computations (a) $Re_D = 3,000$ (b) $Re_D = 10,000$ (c) $Re_D = 30,000$.

519 not correctly reproduced, especially the size of the recirculation regions behind
 520 the pins, as seen and discussed before. It is also observed that for these models
 521 separation was delayed, which led to a weak prediction downstream of the pins.
 522 This can also be seen in the contour plots of the mean stream-wise velocity in
 523 Fig. 6. On the other hand, the ϕ -model comparisons are somewhat better for the
 524 deeper rows. It can, however, be noticed that at the highest Reynolds number
 525 the pressure recovery in general is not predicted very accurately by all the tested
 526 models; in addition to the local separation and reattachment, the strong vortex
 527 shedding from the sides of the pins make this condition the most difficult to predict
 528 with even the most advanced of the RANS closures.

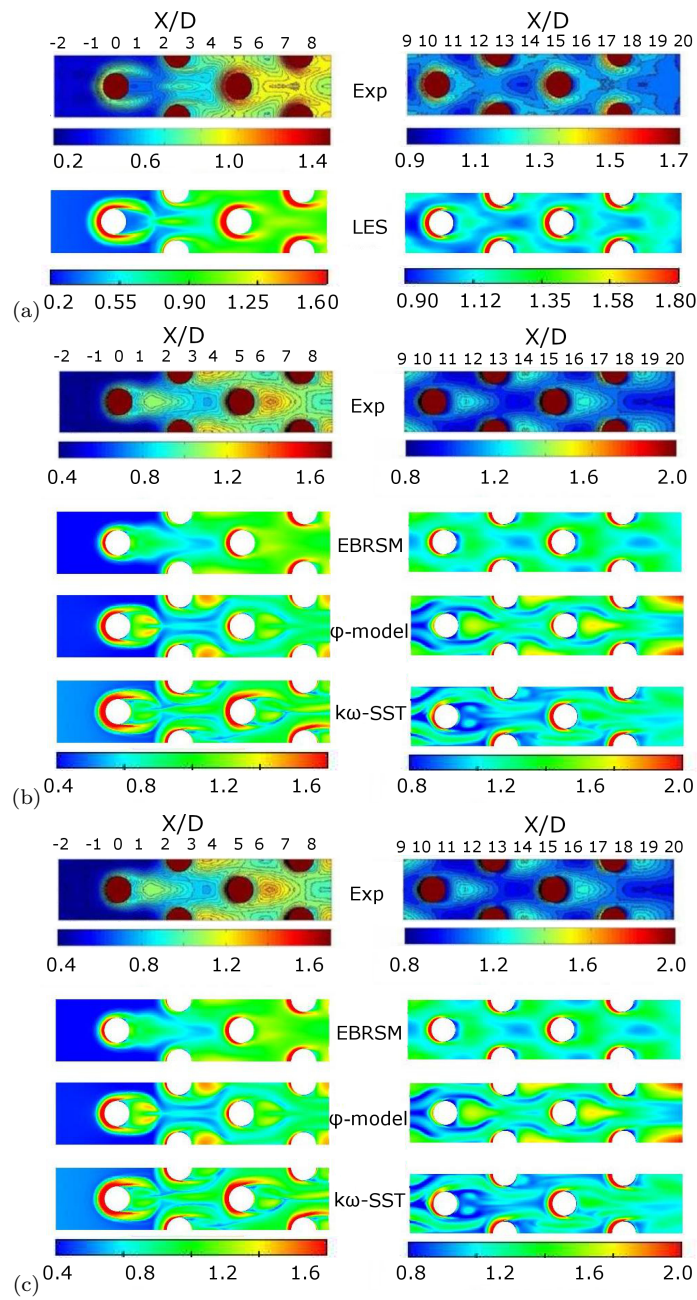


Fig. 13 Comparisons of the Local Nusselt number normalized by its average (Nus/Nus_{av}) (a) $Re_D = 3,000$ (b) $Re_D = 10,000$ (c) $Re_D = 30,000$.

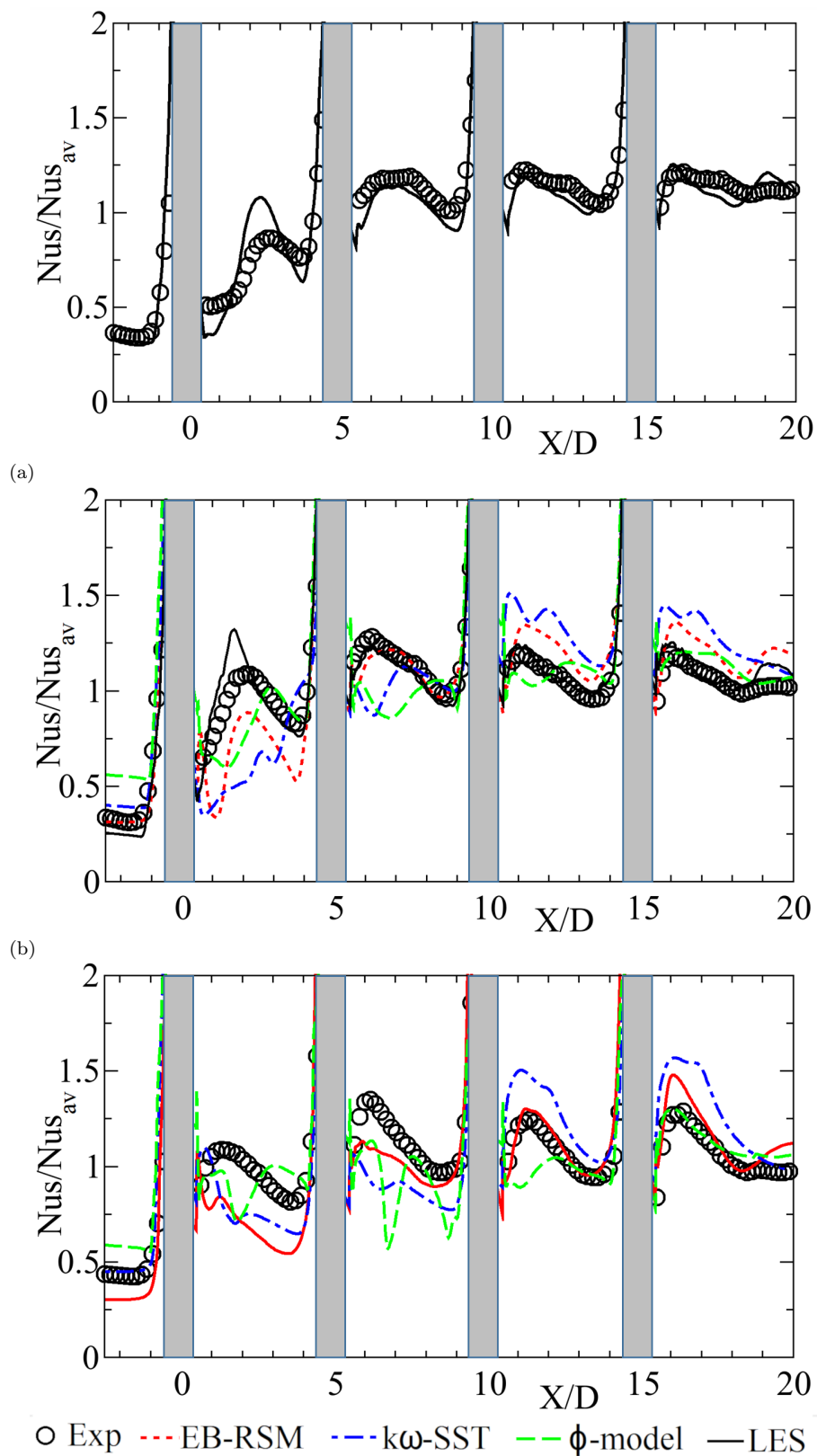


Fig. 14 Local Nusselt number normalized by its average (Nus/Nus_{av}) at mid-span $Y/D = 0$ plane (a) $Re_D = 3,000$ (b) $Re_D = 10,000$ (c) $Re_D = 30,000$.

529 5.4 Nusselt number on the bottom wall

530 Figure 13 shows the contours of the Nusselt number normalized by its average value
531 over the bottom wall. LES computations exhibit an excellent behavior compared
532 to the experimental results. The Nusselt number seems however overestimated at
533 the locations of the horseshoe vortices and underestimated in the wake of the third
534 row, in particular for the highest Reynolds number case. Recall here that the errors
535 made on the average of the normalized Nusselt number were equal to 3% and 1%
536 for the $Re_D = 3,000$ and $Re_D = 10,000$ cases, respectively.

537 For the two eddy-viscosity models, owing to the misprediction of the flow topol-
538 ogy and the fluctuation level observed in previous sections, it is not surprising that
539 both these models cannot predict the local quantities such as the Nusselt number
540 properly. Moreover, it can be observed that for the $k-\omega$ -SST model, the contours
541 are not fully symmetrical, even with a very long averaging time, which suggests
542 the presence of very low frequencies that are probably not physical. On the other
543 hand, the EB-RSM model exhibits a very satisfactory global behavior in particular
544 at the highest Reynolds number. However, the Nusselt number is underestimated
545 in the wake of the first cylinder as the unsteadiness is lower than that predicted
546 by the LES. The prediction for the next rows is satisfactory although an overesti-
547 mation of the heat transfer in the wake of the cylinders was observed for the last
548 4 rows.

549 Figure 14 shows the detailed profiles of the normalized Nusselt number at mid-
550 span ($Y/D = 0$ plane). LES exhibits very good results in general, except in the
551 wake of the first pin, where roughly halfway between the two pins, the maximum
552 of the Nusselt number is overestimated for both the tested Reynolds numbers. The
553 Nusselt number is also underestimated just after each pin, but this discrepancy is
554 present for all the models and at all the tested Reynolds numbers. This suggests
555 that the underestimation is not due to the turbulence modelling but rather due to
556 the use of adiabatic conditions on the pin walls, which is not fully representative
557 of the experimental setup.

558 The results provided by the URANS models are mixed. Clearly, the $k-\omega$ -SST
559 is the least satisfactory model, since the results do not match the experiments
560 anywhere. In the wake of the first pin, where turbulence is not yet fully developed,
561 mixing is dominated by the large-scale unsteadiness, which is not reproduced by
562 this model. In contrast, in the wake of the last two pins, turbulence has developed,
563 as seen in Fig. 9, and the model overestimates turbulent mixing and heat transfer.
564 The ϕ -model better reproduces the Nusselt number in the wake of the last pin,
565 but, in accordance with what has been said earlier, the model does not reproduce
566 the large-scale unsteadiness either, such that the mixing of momentum and heat is
567 underestimated in the wakes of the first few pins. On the other hand the behaviour
568 of the EB-RSM is globally comparable to that of LES, although after the first row,
569 the Nusselt number is significantly underestimated.

570 **6 Conclusions**

571 Simulations were carried out for the flow through a wall-bounded pin matrix in a
572 staggered arrangement with an imposed heat flux at the bottom wall, at various

573 Reynolds numbers (3,000, 10,000, 30,000) based on the gap velocity and the di-
574 ameter of the pins. Two LES simulations (with 18 and 76 million computational
575 cells) and six URANS simulations (utilizing 17 and 29 million cells) were per-
576 formed. For URANS, the ϕ -model, k - ω -SST model (both associated to the SGDH
577 with a constant turbulent Prandtl number) and the EB-RSM model combined
578 to the GGDH were used. For LES, the dynamic Smagorinsky model with Lilly's
579 minimization was used. Both global and local comparisons were drawn against
580 experimental data of Ames et al. and hybrid model simulations of Delibera et al.

581 A global evaluation of the results was performed by computing pressure loss
582 coefficients and average Nusselt numbers. For a more detailed evaluation, the mean
583 pressure coefficient, the mean velocity profiles, *r.m.s.* of stream-wise velocity, re-
584 solved and modelled contributions to *r.m.s.* values and the Nusselt number at the
585 bottom wall were computed for all the models.

586 For the global pressure loss coefficient, LES at $Re_D = 3,000$ and $Re_D =$
587 $10,000$ exhibited excellent comparisons with both experimental and analytical
588 correlations. For the URANS models, it was observed that only the EB-RSM model
589 produced reliable results but only for $Re_D = 10,000$. For the higher Re_D case of
590 $30,000$ none of the models seems to perform particularly well; the worst results
591 were obtained by the eddy-viscosity models. For the average Nusselt number the
592 current LES and EB-RSM results were again found to be in good agreement with
593 the experiments for all the tested Re_D numbers. Once again, the two eddy-viscosity
594 models did not provide accurate results mainly due to their inability to reproduce
595 the unsteadiness of the flow.

596 The detailed comparison of the results with the experiments and amongst the
597 models is particularly interesting and the complete set of results can be accessed via
598 the ERCOFTAC-KB-Wiki. It is observed that the models fall into two categories:
599 those which are able to reproduce the unsteadiness of the wakes of the pins (LES
600 and EB-RSM) and those which essentially provide a steady solution, at least for
601 the first few rows (eddy-viscosity models). The correct reproduction of the global
602 topology of the flow, in particular the length of the recirculation regions behind the
603 pins, is closely related to the presence of a major unsteady contribution. This can
604 be traced to the fact that the turbulent/unsteady structures which efficiently mix
605 momentum in the wake of bluff bodies are the very large-scale structures, which
606 are resolved by LES and EB-RSM, but not by the eddy-viscosity models. This is in
607 line with several previous studies, such as Durbin (1995) or Iaccarino et al. (2003),
608 in which it was shown that the pure RANS models, i.e., RANS models used in a
609 steady-state computation, are not able to correctly reproduce such wakes, while
610 the same models used in URANS mode, i.e., in a time-dependent computation,
611 provide excellent results.

612 Consequently, reproducing the characteristics of pin-fin-array flows, in which
613 each row of pins is affected by the wake of the preceding row, requires a time-
614 dependent computation in which the unsteadiness develops rapidly, starting from
615 the first row. This behavior is not only observed for LES, but also for the Reynolds-
616 stress model, for which the mixing is dominated by the resolved contribution. In
617 contrast, EVM models face strong difficulties to develop unsteadiness at the first
618 few rows, which severely affects the global predictions. Following previous studies
619 (Hadžić et al. 2001; Carpy and Manceau 2006; Hamlington and Dahm 2009), this
620 issue can be related to the misalignment of the Reynolds-stress and mean strain
621 tensors in non-equilibrium flows (stress-strain lag), such as cylinder wakes, which

is ignored by the eddy-viscosity models; the resulting overestimation of modelled turbulence energy in the wake prevents the development of resolved unsteadiness.

In conclusion, for such a complex configuration, consisting of a staggered arrangement of wall-mounted obstacles, with heat transfer, LES can provide accurate and reliable solutions. URANS can provide an alternative solution, particularly attractive for high Reynolds numbers, for which LES can become prohibitively costly, but the choice of the RANS closure is crucial. Due to the importance of avoiding an overestimation of turbulent diffusion in the wakes of the pins, eddy-viscosity models should be avoided and a Reynolds-stress model, or, possibly, a lag eddy-viscosity model (Revell et al. 2011), should be used. For this case, in the forced convection regime, the model for the turbulent heat fluxes is not crucial; associated with the EB-RSM, which globally provides accurate flow dynamics, the Generalized Gradient Diffusion Hypothesis (GGDH) appears sufficient to reproduce the main heat transfer characteristics.

Acknowledgements The authors would like to thank *Électricité de France (eDF)* for the computational resources and Prof. Forrest Ames for providing the experimental data for comparisons. The authors would also like to thank Prof. Wolfgang Rodi for his thoughtful review of the test case for the ERCOFTAC KB-CFD Wiki and his invaluable comments about the present article.

Compliance with Ethical Standards: The authors declare that they have no conflict of interest.

References

- I. Afgan, Y. Kahil, S. Benhamadouche, P. Sagaut, Large eddy simulation of the flow around single and two side-by-side cylinders at subcritical reynolds numbers. *Physics of Fluids* **23**(7), 075101 (2011). doi:10.1063/1.3596267
- I. Afgan, C. Moulinec, R. Prosser, D. Laurence, Large eddy simulation of turbulent flow for wall mounted cantilever cylinders of aspect ratio 6 and 10. *International Journal of Heat and Fluid Flow* **28**(4), 561–574 (2007). Including Special Issue of Conference on Modelling Fluid Flow (CMFF'06), Budapest. doi:https://doi.org/10.1016/j.ijheatfluidflow.2007.04.014
- M.M. Alam, Y. Zhou, Flow around two side-by-side closely spaced circular cylinders. *Journal of Fluids and Structures* **23**(5), 799–805 (2007). doi:https://doi.org/10.1016/j.jfluidstructs.2006.12.002
- M.M. Alam, M. Moriya, H. Sakamoto, Aerodynamic characteristics of two side-by-side circular cylinders and application of wavelet analysis on the switching phenomenon. *Journal of Fluids and Structures* **18**(3), 325–346 (2003). Bluff-body/Flow interactions. doi:https://doi.org/10.1016/j.jfluidstructs.2003.07.005
- F.E. Ames, L.A. Dovrak, The Influence of Reynolds Number and Row Position on Surface Pressure Distributions in Staggered Pin Fin Arrays, in *ASME. Turbo Expo: Power for Land, Sea, and Air*, vol. 3: Heat Transfer, Parts A and B, 2006a, pp. 149–159. doi:10.1115/GT2006-90170
- F.E. Ames, L.A. Dovrak, Turbulent transport in pin fin arrays: Experimental data and predictions. *ASME. J. Turbomach* **128**(1), 71–81 (2006b). doi:10.1115/1.2098792
- F.E. Ames, L.A. Dvorak, M.J. Morrow, Turbulent augmentation of internal convection over pins in staggered pin fin arrays. *ASME. J. Turbomach* **127**, 183–190 (2005)
- F.E. Ames, C.A. Nordquist, L.A. Klennert, Endwall Heat Transfer Measurements in a Staggered Pin Fin Array With an Adiabatic Pin, in *ASME. Turbo Expo: Power for Land, Sea, and Air*, vol. 4: Turbo Expo 2007, Parts A and B, 2007, pp. 423–432. doi:10.1115/GT2007-27432

- 671 F. Archambeau, N. Mechtoua, M. Sakiz, Code_saturne: A finite volume code for the
672 computation of turbulent incompressible flows - industrial applications. *Int. J. Finite Vol.*
673 **1**(1) (2004)
- 674 J. Armstrong, D. Winstanley, A review of staggered array pin fin heat transfer for turbine
675 cooling applications. *ASME-Journal of Turbomachinery* **110**(1), 94–103 (1988)
- 676 A. Arshad, H.M. Ali, S. Khushnood, M. Jabbal, Experimental investigation of pcm based
677 round pin-fin heat sinks for thermal management of electronics: Effect of pin-fin
678 diameter. *International Journal of Heat and Mass Transfer* **117**, 861–872 (2018).
679 doi:<https://doi.org/10.1016/j.ijheatmasstransfer.2017.10.008>
- 680 M. Axtmann, R. Poser, J. von Wolfersdorf, M. Bouchez, Endwall heat transfer and pressure
681 loss measurements in staggered arrays of adiabatic pin fins. *Applied Thermal Engineering*
682 **103**, 1048–1056 (2016). doi:<https://doi.org/10.1016/j.applthermaleng.2016.04.066>
- 683 S. Benhamadouche, Large eddy simulation with the unstructured collocated arrangement,
684 PhD thesis, Ph.D. thesis, The University of Manchester, 2006. TH28140
- 685 S. Benhamadouche, F. Dehoux, I. Afgan, Unsteady RANS and Large Eddy Simulation of the
686 flow and heat transfer in a wall bounded pin matrix, in *ICHMT. In Proceedings*
687 *Turbulence, Heat and Mass Transfer 7 - Palermo, Italy*, 2012, pp. 1624–1634.
688 doi:10.1615/ICHMT.2012.ProcSevIntSympTurbHeatTransfPal.1670
- 689 S. Carpy, R. Manceau, Turbulence modelling of statistically periodic flows: synthetic jet into
690 quiescent air. *Int. J. Heat Fluid Fl.* **27**, 756–767 (2006)
- 691 F. Dehoux, Y. Lecocq, S. Benhamadouche, R. Manceau, L.-E. Brizzi, Algebraic modeling of
692 the turbulent heat fluxes using the elliptic blending approach—application to forced and
693 mixed convection regimes. *Flow, Turbulence and Combustion* **88**(1), 77–100 (2012).
694 doi:10.1007/s10494-011-9366-8
- 695 G. Delibra, D. Borello, K. Hanjalić, F. Rispoli, LES of flow and heat transfer in a channel
696 with a staggered cylindrical pin matrix., in *Direct and Large-Eddy Simulation VII. Inter.*
697 *ERCOFTAC Workshop on Direct and Large-Eddy Simulation ERCOFTAC Series,*
698 *Springer, 2010*, vol. 7, ISBN: 978-90-481-3651-3, 2008
- 699 G. Delibra, D. Borello, K. Hanjalić, F. Rispoli, Urans of flow and endwall heat transfer in a
700 pinned passage relevant to gas-turbine blade cooling. *International Journal of Heat and*
701 *Fluid Flow* **30**(3), 549–560 (2009). The Seventh International Symposium on Engineering
702 Turbulence Modelling and Measurements, ETMM7.
703 doi:<https://doi.org/10.1016/j.ijheatfluidflow.2009.03.015>
- 704 G. Delibra, K. Hanjalić, D. Borello, F. Rispoli, Vortex structures and heat transfer in a
705 wall-bounded pin matrix: Les with a rans wall-treatment. *International Journal of Heat*
706 *and Fluid Flow* **31**(5), 740–753 (2010). Sixth International Symposium on Turbulence,
707 Heat and Mass Transfer, Rome, Italy, 14-18 September 2009.
708 doi:<https://doi.org/10.1016/j.ijheatfluidflow.2010.03.004>
- 709 P.A. Durbin, Near-wall turbulence closure modeling without “damping functions”.
710 *Theoretical and Computational Fluid Dynamics* **3**(1), 1–13 (1991).
711 doi:10.1007/BF00271513
- 712 P.A. Durbin, Separated flow computations with the k-epsilon-v-squared model. *AIAA*
713 *Journal* **33**(4), 1–13 (1995). doi:10.2514/3.12628
- 714 P.A. Durbin, On the k -3 stagnation point anomaly. *Int. J. Heat Fluid Fl.* **17**(1), 89–90 (1996)
- 715 A. Fadai-Ghotbi, R. Manceau, J. Borée, Revisiting urans computations of the
716 backward-facing step flow using second moment closures. influence of the numerics. *Flow,*
717 *Turbulence and Combustion* **81**(3), 395–414 (2008). doi:10.1007/s10494-008-9140-8
- 718 J.H. Ferziger, M. Perić, *Computational Methods for Fluid Dynamics*, (Springer Berlin
719 Heidelberg, Berlin, 2012). ISBN 9783642560262
- 720 J. Frohlich, C.P. Mellen, W. Rodi, L. Temmerman, M.A. Leschziner, Highly resolved
721 large-eddy simulation of separated flow in a channel with streamwise periodic
722 constrictions. *Journal of Fluid Mechanics* **526**, 19–66 (2005).
723 doi:10.1017/S0022112004002812
- 724 M. Germano, U. Piomelli, P. Moin, W.H. Cabot, A dynamic subgrid scale eddy viscosity
725 model. *Physics of Fluids A: Fluid Dynamics* **3**(7), 1760–1765 (1991).
726 doi:10.1063/1.857955
- 727 G. Grotzbach, Revisiting the resolution requirements for turbulence simulations in nuclear
728 heat transfer. *Nuclear Engineering and Design* **241**(11), 4379–4390 (2011). 13th
729 International Topical Meeting on Nuclear Reactor Thermal Hydraulics (NURETH-13).
730 doi:<https://doi.org/10.1016/j.nucengdes.2010.12.027>

- 731 I. Hadžić, K. Hanjalić, D. Laurence, Modeling the response of turbulence subjected to cyclic
732 irrotational strain. *Phys. Fluids* **13**(6), 1739–1747 (2001)
- 733 P.E. Hamlington, W.J.A. Dahm, Frequency response of periodically sheared homogeneous
734 turbulence. *Phys. Fluids* **21**(5), 1–11 (2009)
- 735 K. Hanjalić, D.R. Laurence, M. Popovac, J.C. Uribe, Turbulence Model and Its Application
736 to Forced and Natural Convection, in *Engineering Turbulence Modelling and*
737 *Experiments 6*, ed. by W. Rodi, M. Mulas (Elsevier Science B.V., Amsterdam, 2005), pp.
738 67–76. ISBN 978-0-08-044544-1. doi:<https://doi.org/10.1016/B978-008044544-1/50005-4>
- 739 L. Huang, Q. Li, H. Zhai, Experimental study of heat transfer performance of a tube with
740 different shaped pin fins. *Applied Thermal Engineering* **129**, 1325–1332 (2018).
741 doi:<https://doi.org/10.1016/j.applthermaleng.2017.10.014>
- 742 S.-C. Huang, C.-C. Wang, Y.-H. Liu, Heat transfer measurement in a rotating cooling
743 channel with staggered and inline pin-fin arrays using liquid crystal and stroboscopy.
744 *International Journal of Heat and Mass Transfer* **115**, 364–376 (2017).
745 doi:<https://doi.org/10.1016/j.ijheatmasstransfer.2017.07.040>
- 746 G. Iaccarino, A. Ooi, P.A. Durbin, M. Behnia, Reynolds averaged simulation of unsteady
747 separated flow. *Int. J. Heat Fluid Fl.* **24**, 147–156 (2003)
- 748 M. Jacob, Heat Transfer and Flow Resistance in Cross Flow of Gases Over Tube Banks, in
749 *Trans. ASME*, vol. 59, 1938, pp. 384–386
- 750 S. Lardeau, M.A. Leschziner, Unsteady RANS modelling of wake-blade interaction:
751 computational requirements and limitations. *Comput. Fluids* **34**, 3–21 (2005)
- 752 D.R. Laurence, J.C. Uribe, S.V. Utyuzhnikov, A robust formulation of the v2-f model. *Flow,*
753 *Turbulence and Combustion* **73**(3), 169–185 (2005). doi:10.1007/s10494-005-1974-8
- 754 W. Li, L. Yang, J. Ren, H. Jiang, Effect of thermal boundary conditions and thermal
755 conductivity on conjugate heat transfer performance in pin fin arrays. *International*
756 *Journal of Heat and Mass Transfer* **95**, 579–592 (2016).
757 doi:<https://doi.org/10.1016/j.ijheatmasstransfer.2015.12.010>
- 758 D.K. Lilly, A proposed modification of the germano subgrid-scale closure method. *Physics of*
759 *Fluids A: Fluid Dynamics* **4**(3), 633–635 (1992). doi:10.1063/1.858280
- 760 R. Manceau, K. Hanjalić, Elliptic blending model: A new near-wall reynolds-stress
761 turbulence closure. *Physics of Fluids* **14**(2), 744–754 (2002). doi:10.1063/1.1432693
- 762 R. Manceau, Recent progress in the development of the elliptic blending reynolds-stress
763 model. *International Journal of Heat and Fluid Flow* **51**, 195–220 (2015). Theme special
764 issue celebrating the 75th birthdays of Brian Launder and Kemo Hanjalic.
765 doi:<https://doi.org/10.1016/j.ijheatfluidflow.2014.09.002>.
766 <http://www.sciencedirect.com/science/article/pii/S0142727X14001179>
- 767 F.R. Menter, Two-equation eddy-viscosity turbulence models for engineering applications.
768 *AIAA Journal* **32**(8), 1598–1605 (1994)
- 769 F.R. Menter, M. Kuntz, R. Langtry, Ten years of industrial experience with the SST
770 turbulence model, in *Proc. 4th Int. Symp. Turbulence, Heat and Mass Transfer,*
771 *Antalya, Turkey, 2003*
- 772 D.E. Metzger, Z.X. Fan, W.B. Shepard, Pressure loss and heat transfer through multiple
773 rows of short pin fins, in *Heat Transfer 1982, Volume 3*, vol. 3, 1982, pp. 137–142
- 774 C.A. Nordquist, Pin Fin End Wall Heat Transfer Distributioin with an Adiabatic Pin
775 Acquired using an Infrared Camera., in *Master of Science Thesis, the University of*
776 *North Dakota*, 2006
- 777 P. Parnaudeau, J. Carlier, D. Heitz, E. Lamballais, Experimental and numerical studies of
778 the flow over a circular cylinder at reynolds number 3900. *Physics of Fluids* **20**(8),
779 085101 (2008). doi:10.1063/1.2957018
- 780 M. Qian, D. Mei, Z. Yi, Y. Feng, Z. Chen, Fluid flow and heat transfer performance in a
781 micro-reactor with non-uniform micro-pin-fin arrays for hydrogen production at low
782 reynolds number. *International Journal of Hydrogen Energy* **42**(1), 553–561 (2017).
783 doi:<https://doi.org/10.1016/j.ijhydene.2016.10.150>
- 784 Y. Rao, Y. Xu, C. Wan, An experimental and numerical study of flow and heat transfer in
785 channels with pin fin-dimple and pin fin arrays. *Experimental Thermal and Fluid Science*
786 **38**, 237–247 (2012). doi:<https://doi.org/10.1016/j.exptthermflusci.2011.12.012>
- 787 A.J. Revell, T.J. Craft, D.R. Laurence, Turbulence modelling of unsteady turbulent flows
788 using the stress strain lag model. *Flow, Turb. and Combust.* **86**(1), 129–151 (2011)
- 789 C.M. Rhie, W.L. Chow, A numerical study of the turbulent flow past an isolated airfoil with
790 training edge separation. *AIAA paper* (1982)

- 791 E.M. Sparrow, J.W. Ramsey, C.A.C. Altemani, Experiments on in-line pin fin arrays and
792 performance comparisons with staggered arrays. *J. Heat Transfer* **102**(1), 44–50 (1980).
793 doi:10.1115/1.3244247
- 794 C.G. Speziale, S. Sarkar, T.B. Gatski, Modelling the pressure–strain correlation of
795 turbulence: an invariant dynamical systems approach. *Journal of Fluid Mechanics* **227**,
796 245–272 (1991). doi:10.1017/S0022112091000101
- 797 D.B. Taulbee, L. Tran, Stagnation streamline turbulence. *AIAA J.* **26**(8), 1011–1013 (1988)
- 798 L. Temmerman, M.A. Leschziner, C.P. Mellen, J. Frohlich, Investigation of wall-function
799 approximations and subgrid-scale models in large eddy simulation of separated flow in a
800 channel with streamwise periodic constrictions. *International Journal of Heat and Fluid*
801 *Flow* **24**(2), 157–180 (2003). doi:https://doi.org/10.1016/S0142-727X(02)00222-9
- 802 G.J. VanFossen, Heat Transfer Coefficients for Staggered Arrays of Short Pin Fins, in *Turbo*
803 *Expo: Power for Land, Sea, and Air*, vol. Volume 3: Heat Transfer; Electric Power, 1981
- 804 P.-L. Violette, J.-P. Chabard, P. Esposito, D. Laurence, *Mécanique des fluides appliquée*
805 (Presses de l'école nationale des ponts et chaussées, Paris, 1998)
- 806 M.M. Zdravkovich, *Flow Around Circular Cylinders, Fundamentals*, (Oxford University
807 Press, New York, 1997). ISBN 9780198563969